PAPER • OPEN ACCESS

The role of bridge nodes between layers on epidemic spreading

To cite this article: L D Valdez *et al* 2018 *New J. Phys.* **20** 125003

View the article online for updates and enhancements.

New Journal of Physics

The open access journal at the forefront of physics

Deutsche Physikalische Gesellschaft **DPG**

IOP Institute of Physics

Published in partnership with: Deutsche Physikalische Gesellschaft and the Institute of Physics

CrossMark

PAPER

The role of bridge nodes between layers on epidemic spreading

L D Valdez[1], H H Aragão Rêgo[2], H E Stanley[1], S Havlin[3] and L A Braunstein[4,1]

[1] Center for Polymer Studies, Boston University, Boston, MA 02215, United States of America
[2] Departamento de Física, Instituto Federal de Educação Tecnológica do Maranhão, São Luís, MA, 65030-005, Brazil
[3] Department of Physics, Bar-Ilan University, Ramat-Gan 52900, Israel
[4] Instituto de Investigaciones Físicas de Mar del Plata (IFIMAR)-Departamento de Física, Facultad de Ciencias Exactas y Naturales, Universidad Nacional de Mar del Plata-CONICET, Funes 3350, (7600) Mar del Plata, Argentina

E-mail: ldvaldez@bu.edu

Abstract

Real networks, like the international airport network and the Internet, are composed of interconnected layers (or communities) through a small fraction of nodes that we call here 'bridge nodes'. These nodes are crucial in the spreading of epidemics because they enable the spread the disease to the entire system. In this work we study the effect of the bridge nodes on the susceptible-infected-recovered model in a two layer network with a small fraction r of these nodes. In the dynamical process, we theoretically determine that at criticality and for the limit $r \rightarrow 0$, the time t_b at which the first bridge node is infected diverges as a power-law with r, while above criticality, it appears a crossover between a logarithmic and a power-law behavior. Additionally, in the steady state at criticality, the fraction of recovered nodes scales with r as a power-law whose exponent can be understood from the finite size cluster distribution at criticality. We also test our model on the real international airline network and show that 'high-degree bridge nodes' reduce the time t_b.

1. Introduction

One of the main aspects of the spread of contagious diseases in society, such as the Influenza [1], Ebola [2], and syphilis [3] is that these processes rely not only on the pathogen-specific characteristics but also on the structure of the network of interactions among individuals. Consequently, in the last two decades, many researchers have studied the effect of the structure of complex networks on the spread of epidemics, in order to improve the epidemic forecast and to propose efficient strategies to mitigate their effects on the population [4, 5]. Initially, most researches have focused on isolated networks, but in the recent years, in particular, since 2010 [6] multilayer networks or network-of-networks (NON) attracted much interest, since they are more general and suitable to model more realistic interactions between people. In a NON, the nodes in a network which interact with nodes in other networks are called here 'bridge nodes' [7] and the links that connect bridge nodes of different networks are called 'external links'. On the other hand, within each layer, all the nodes (including the bridge ones) are connected by internal links. One of the most fundamental microscopic measures that characterize the topology or internal structure of a network is the degree distribution $P(k)$, which is the fraction of nodes with k internal contacts within the same network [8]. A particular class of NON is the multilayer networks [9, 10] in which a fraction $r \leqslant 1$ of nodes are bridge nodes in each network or layer, and each of these nodes are connected or 'interacts' with only one bridge node in the other layers [11]. This structure that we call a simple multilayer network, is suitable for example, for modeling the propagation of a rumor in which an individual can transmit the rumor both in a virtual layer (for example Facebook) and in a physical network or layer of face-to-face contact [12]. The individual who participates in both layers is represented by a bridge node in each layer, which is connected to each other through an external link. Several studies showed that simple multilayer networks boost the propagation of information [12], accelerate diffusion processes [13], delay reactions [14] and increase the virulence of diseases with respect to an isolated network [15].

In the last two decades, several mathematical models have been developed using complex networks as a substrate to describe the spread of diseases [4, 16, 17]. One of the most studied models is the Susceptible-Infected-Recovered (SIR) which is suitable for diseases that confer permanent immunity [18]. In this model, initially each node is in the susceptible state (*S*), that is, it is healthy but not immunized to the disease, except for an infected individual (*I*), which is called the index case. Each individual in state *I* can transmit the disease to his/her contacts in state *S* with probability β during a time t_r since he/she became infected. After that period, the individual *I* goes to the recovered state (*R*) and stops transmitting the disease. The epidemics continues spreading until it reaches the steady state in which there are no more infected individuals. Depending on the context, we also refer to *S*, *I* and *R* as the fraction of susceptible, infected and recovered individuals, respectively. One of the main features of this model in the steady state, is that it undergoes a second order phase transition between two regimes that are governed by the transmissibility *T* [19]. This quantity represents the effective probability of contagion, given by $T = 1 - (1 - \beta)^{t_r}$ and it is the control parameter of the transition. This transition occurs at a critical value $T = T_c$ which depends on the topology of the system. On the other hand, the order parameter of the system is the fraction of recovered individuals *R* in the steady state. It is known that in isolated networks as well as in simple multilayer networks, the SIR model in the steady state can be exactly mapped onto link percolation [15, 19, 20]. In this framework, the fraction of recovered nodes *R* is analogous to the fraction of nodes in the giant component (GC), and *T* plays the role of the probability *p* of link occupation. In isolated single networks, there is only one single component or cluster of recovered nodes in the steady state. Similarly, in simple multilayer networks, there is only one cluster of recovered nodes, formed by both internal and external links that are used to transmit the disease [15].

Although the spread of diseases in simple multilayer networks has been extensively investigated in recent years, the effect of bridge nodes with multiple external links has received little attention. On the other hand, in some real multilayer networks, there are usually few bridge nodes in each layer and in turn they have many external connections compared to the average degree in their layer. This kind of structure appears when only few nodes in one layer have sufficient infrastructure, and the necessary economic and human resources to connect with nodes in other layers. For example, in some social networks, only a few individuals of one community or layer may have the necessary skills to establish commercial and cultural relationships with individuals from other layers [21]. In another example, in a national and international airport network, most of the airports in a country (layer) only serve national flights, while a small set of airports serve international flights from and to other countries (layers) [22]. One additional feature of these international airports (bridge nodes) is that they may have many external links, i.e. flights to many nodes in other layers since they have the necessary infrastructure to support the air traffic to and from many countries. These bridge nodes with a large number of external links are called 'central bridge nodes', which could be considered as influential spreaders or superspreaders [23–25]. Hereafter, for simplicity, we will refer to the 'central bridge nodes' as 'bridge nodes'. This type of structure is more general than the simple multilayer model[5]. Very recently, Dong *et al* [11] studied a node percolation process on this structure and obtained that the fraction of nodes in the GC behaves as a power law with the fraction of bridge nodes *r*, which is analogous to the relation between the magnetization and the external field in the Ising model.

In this work, we study the SIR model in a two-layered network with a fraction *r* of central bridge nodes during the dynamic process and in the steady state. In section 2 we present our model and the dynamic equations. In sections 3 and 4 we show the scaling properties of the time t_b at which the disease reaches the first bridge node. In section 5 we focus on the steady state of the epidemic process at criticality, i.e. at the critical point and explain how the structure of the recovered clusters explains the scaling relation between the fraction of recovered nodes and the fraction of bridge nodes. In section 6 we apply our model to real flight networks. Finally in section 7 we present our conclusions.

2. Model and dynamic equations

In this paper we study the SIR model in a system of two layers or networks with the same number of nodes *N*, in which a fraction *r* of nodes in each layer are 'bridge nodes', that is, they have external links which connect to bridge nodes in the other layer. Additionally, we consider that the external connectivity follows a Poisson or Erdös Rényi (ER) distribution with a mean external connectivity equal to $\langle k_{ext} \rangle = c/r$, where *c* is a constant. This implies that $r \langle k_{ext} \rangle = c$, so the total number of external links M_I is constant and equal to *cN*. The Poisson distribution in the external connectivity will allow us to study the effect of an increasing mean external

---

[5] Note that the structure of our model with two layers can be interpreted as a network with two communities. Heuristically, a community is a subnetwork in which the density of its internal links is greater than its external links. However, since in our model the number of external links could be comparable to the number of internal links, we prefer to use the term of layers and multilayer networks, instead of network with communities.

connectivity while the number of external links is constant. Unless otherwise indicated, the bridge nodes are chosen randomly and the external links only connect bridge nodes from different layers. The nodes that do not have external links are called 'internal nodes'. In the main text of this work, we present our results for $M_I = N$, but in the appendix the reader can find our results for $M_I < N$. For the stochastic simulations of the SIR model, we randomly choose the index case in one layer, which can be also a bridge node.

In order to study the evolution of the states of the individuals in the SIR with fixed recovery time, we use the edge-based compartmental model (EBCM) [26–28]. In single networks, this approach is based on using two generating functions. The first one is the generating function of the node degree distribution $P(k)$ which is given by $G_0(x) = \sum_k P(k) x^k$, with $k_{\min} \leqslant k \leqslant k_{\max}$. Here, $k_{\min}$ and $k_{\max}$ are the minimum and maximum values of the degree distribution. The second one is the generating function of the degree distribution of the first neighbors of a node, $P_1(k) \equiv kP(k)/\langle k \rangle$, given by $G_1(x) = \sum_k kP(k)/\langle k \rangle x^{k-1}$, where $\langle k \rangle$ is the first moment of $P(k)$. Here, $P_1(k)$ is the probability to reach a neighbor of a node with degree k, following a random chosen link. For simplicity, we will assume in this work that both networks have the same degree distribution in order to reduce the number of equations.

The EBCM approach describes the evolution of the fraction of susceptible ($S(t)$), infected ($I(t)$) and recovered ($R(t)$) individuals at time t by computing an auxiliary probability $\theta(t)$. Note that this approach is only valid in the deterministic regime of the epidemic spreading, that is, when the fluctuations of the number of infected nodes at time t are negligible with respect to the mean number of infected nodes. In a single network, $\theta(t) \equiv \theta_t$ stands for the probability that a randomly chosen node through a link has not transmitted the disease towards this link. This could be due to the following cases:

(i) the node is susceptible with probability $\Phi_S(t)$, so it cannot transmit the disease,

(ii) the node is infected, but it has not transmitted the disease yet, with probability $\Phi_I(t)$.

(iii) the node is recovered and it did not transmit the disease while it was infected, with probability $\Phi_R(t)$.

Therefore, θ_t is given by, $\theta_t = \Phi_S(t) + \Phi_I(t) + \Phi_R(t)$.

Then, given a node with degree k, the probability that none of its neighbors has transmitted the disease to him/her at time t is θ_t^k. If this node is not the index case, i.e. it is not an infected node at the initial condition, then it is in the susceptible state at the beginning of the dynamic process. Since, the fraction of index cases is negligible, then the fraction of susceptible nodes is $S(t) = \sum_k P(k) \theta_t^k = G_0(\theta_t)$ for all t.

Similarly, in a two layer networks with the same degree distribution, the following relations hold: $\theta_t^i = \Phi_S^i(t) + \Phi_I^i(t) + \Phi_R^i(t)$ and $\theta_t^b = \Phi_S^b(t) + \Phi_I^b(t) + \Phi_R^b(t)$, where the magnitudes with a supra-index i and b correspond to the internal and external links or internal and bridge nodes, respectively. Note that the equations do not have an index that indicates the number of the layer because we assume, as mentioned earlier, that both layers have the same degree distribution. Using the EBCM adapted to SIR with fixed t_r, the evolution of $\theta_t^i, \theta_t^b, \Phi_S^i(t), \Phi_S^b(t), \Phi_I^i(t)$ and $\Phi_I^b(t)$ are given by the deterministic equations

$$\theta_{t+1}^i = \theta_t^i - \beta \Phi_I^i(t), \tag{1}$$

$$\theta_{t+1}^b = \theta_t^b - \beta \Phi_I^b(t), \tag{2}$$

$$\Delta \Phi_S^i = (1-r)[G_1^i(\theta_{t+1}^i) - G_1^i(\theta_t^i)] + r[G_1^i(\theta_{t+1}^i)G_0^b(\theta_{t+1}^b) - G_1^i(\theta_t^i)G_0^b(\theta_t^b)], \tag{3}$$

$$\Delta \Phi_S^b = G_0^i(\theta_{t+1}^i)G_1^b(\theta_{t+1}^b) - G_0^i(\theta_t^i)G_1^b(\theta_t^b), \tag{4}$$

$$\Delta \Phi_I^i = -\beta \Phi_I(t)^i - \Delta \Phi_S^i + (1-T)\Delta \Phi_S^i(t-t_r), \tag{5}$$

$$\Delta \Phi_I^b = -\beta \Phi_I(t)^b - \Delta \Phi_S^b + (1-T)\Delta \Phi_S^b(t-t_r), \tag{6}$$

where Δ is the discrete change of the variables between times t and $t+1$. Equation (1) computes the change in θ_t^i when an infected internal node transmits the disease with probability β. Equation (3) represents the change in Φ_S^i when an internal node is infected (first term) and a bridge node is infected (second term). Note that $\Delta \Phi_S(t)^i < 0$. Finally, equation (5) computes the variation of Φ_I^i due to: (i) an infected node transmits the disease which decreases Φ_I^i (first term), (ii) there are new links that lead to the new infected nodes (second term), and (iii) the infected nodes which have not transmitted the disease with probability $1 - T$ during a period t_r, are recovered. Equations (2), (4), and (6) have similar interpretations for the bridge nodes.

Using the equations given above, we can compute the fraction of susceptible and infected nodes as,

$$\Delta S^i = (1-r)[G_0^i(\theta_{t+1}^i) - G_0^i(\theta_t^i)], \tag{7}$$

$$\Delta S^b = r[G_0^i(\theta_{t+1}^i)G_0^b(\theta_{t+1}^b) - G_0^i(\theta_t^i)G_0^b(\theta_t^b)], \tag{8}$$

$$\Delta I^i = -\Delta S^i + \Delta S^i(t-t_r), \tag{9}$$

Figure 1. Time evolution of the total fraction of infected nodes $I = I^i + I^b$, infected internal nodes I^i and infected bridge nodes I^b for two layers with a ER distribution with $\langle k \rangle = 4$, $T = T_c(r = 0) = 0.25$ (this is the critical transmissibility for an isolated network with the same degree distribution), $t_r = 10$ and: (a) $r = 0.20$, (b) $r = 0.05$, and (c) $r = 0.01$. The colored lines correspond to 100 stochastic realizations with $N = 10^5$ for: I (pink), I^i (light blue) and I^b (orange), and the black lines correspond to the theoretical solutions obtained from equations (1)–(10). In the main plot we shifted the time to $t = 0$ when the fraction of total nodes in the infected state is equal to 0.01, in order to compare the theoretical solution with the simulations [26, 28]. In the insets we show 100 stochastic realizations of I (pink) in log-linear scale. In the insets we shifted for each realization, the time to $t = 0$ (indicated by a dashed vertical line) when the first bridge node is infected at time t_b in the simulations.

$$\Delta I^b = -\Delta S^b + \Delta S^b(t - t_r), \tag{10}$$

where $S^i (I^i)$ and $S^b (I^b)$ are the fractions of susceptible (infected) internal and bridges nodes, respectively.
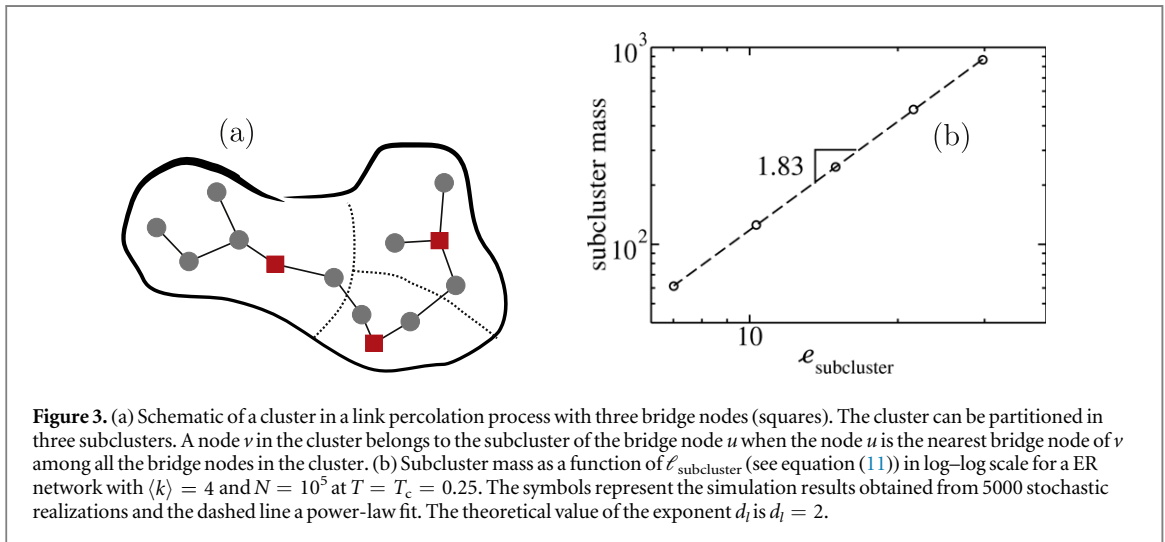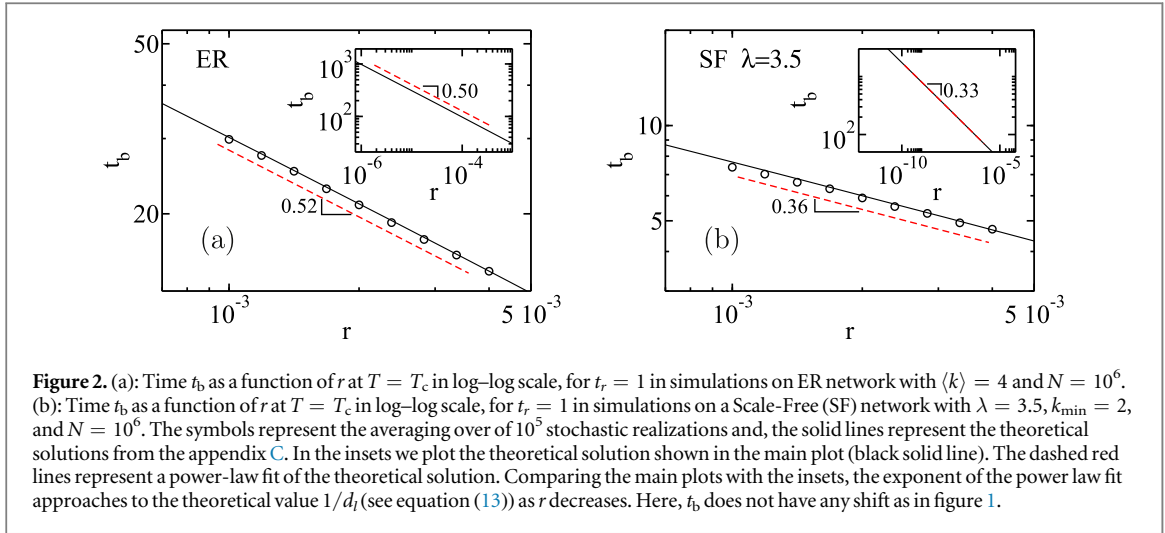
In order to understand the effect of the bridge nodes on the epidemic spreading, in figure 1 we plot the evolution of the fraction of infected internal nodes I^i, infected bridge nodes I^b, and the total fraction of infected nodes $I = I^i + I^b$, for different values of r, at $T = T_c(r = 0) = \langle k \rangle / (\langle k^2 \rangle - \langle k \rangle)$, i.e. at the critical transmissibility value for a single network. Here $\langle k^2 \rangle$ is the second moment of the degree distribution.

From figure 1 we can see that as the fraction of bridge nodes r decreases, a second sharp peak appears in I. This sharp peak is caused by the fast spreading of the infection between the bridge nodes because they have a large connectivity ($\langle k_{\text{ext}} \rangle = 1/r$) and they are connected to each other, so when one bridge node is infected the disease spreads very fast among them. This represents the high vulnerability for disease spreading of international airports during an epidemic spreading. After these nodes are infected, the disease continues spreading to the rest of the network. That is, for very small r, bridge nodes and internal nodes are infected at two different characteristic times, as seen clearly in figure 1(c), since the curve $I(t)$ has two peaks. The first one corresponds to the bridge nodes while the second one to the internal nodes.

From the insets of the figures, we also can see that as r decreases, the disease or epidemics 'explodes' only after the first bridge node is infected at time t_b. This magnitude is also related to the 'arrival time' which is the moment at which the first infected node appears in the other community, metapopulation or layer [7, 29]. Since in such networks, the 'explosion' of the epidemics is governed by the bridge nodes, it is of interest to compute the average time t_b at which the first bridge node is infected, because after that, the fraction of infected nodes will rise very quickly. Unlike our dynamical equations (1)–(10) for the deterministic evolution of the fraction infected nodes which assume that both layers are of the same size, the computation of t_b can be applied to layers of different sizes, because t_b depends only on the topology of the layer in which the disease originates. In the following sections, we will study the dependency of t_b on r for $T = T_c$ and $T \gtrsim T_c$ (note again that T_c is for a single network with $r = 0$).

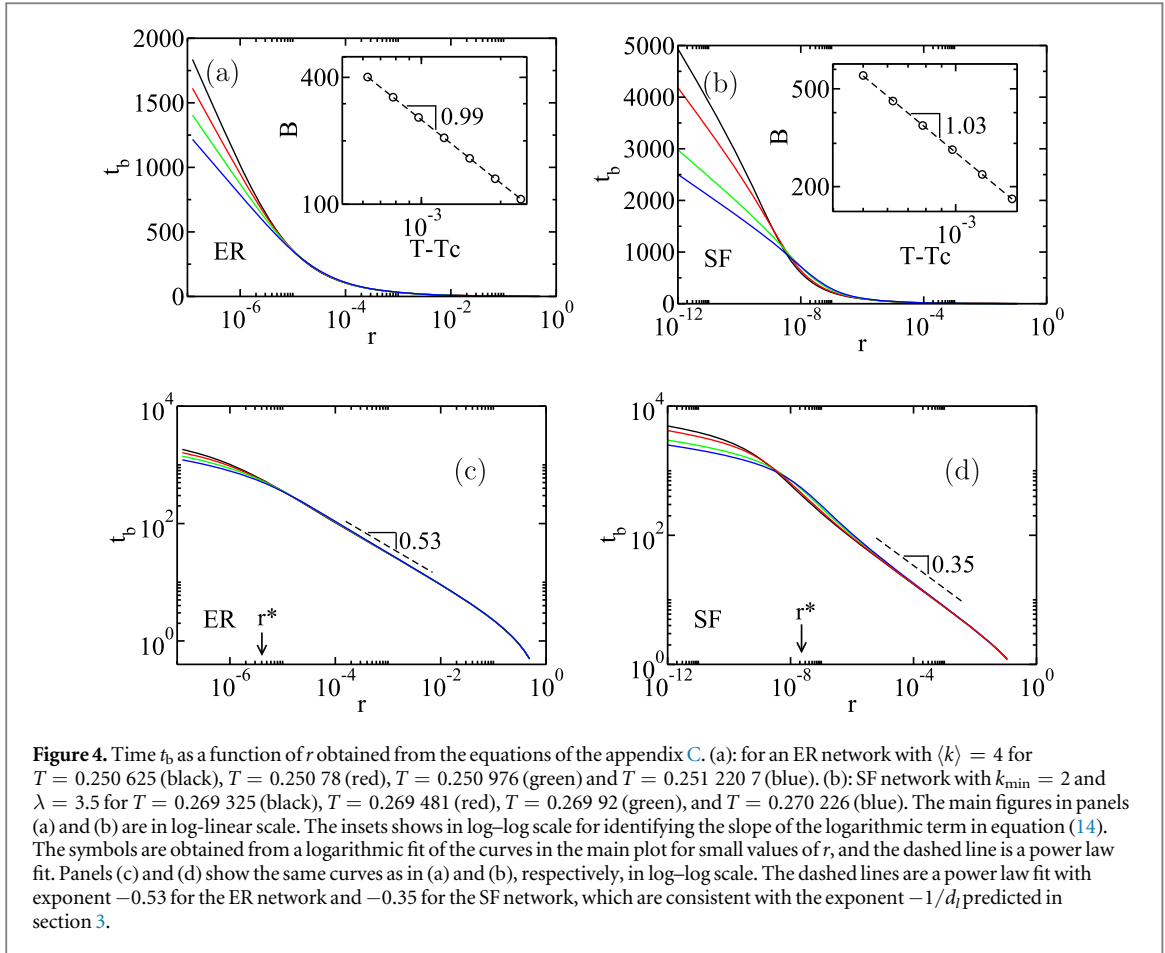## 3. Time to reach the first bridge node t_b at $T = T_c(r = 0)$

In this section we study the relation between t_b and the fraction of bridge nodes, r, when the disease has started in one layer before reaching the other layer. It is important to remark that t_b only depends on the network topology

Figure 2. (a): Time t_b as a function of r at $T = T_c$ in log–log scale, for $t_r = 1$ in simulations on ER network with $\langle k \rangle = 4$ and $N = 10^6$. (b): Time t_b as a function of r at $T = T_c$ in log–log scale, for $t_r = 1$ in simulations on a Scale-Free (SF) network with $\lambda = 3.5$, $k_{min} = 2$, and $N = 10^6$. The symbols represent the averaging over of 10^5 stochastic realizations and, the solid lines represent the theoretical solutions from the appendix C. In the insets we plot the theoretical solution shown in the main plot (black solid line). The dashed red lines represent a power-law fit of the theoretical solution. Comparing the main plots with the insets, the exponent of the power law fit approaches to the theoretical value $1/d_l$ (see equation (13)) as r decreases. Here, t_b does not have any shift as in figure 1.

Figure 3. (a) Schematic of a cluster in a link percolation process with three bridge nodes (squares). The cluster can be partitioned in three subclusters. A node v in the cluster belongs to the subcluster of the bridge node u when the node u is the nearest bridge node of v among all the bridge nodes in the cluster. (b) Subcluster mass as a function of $\ell_{subcluster}$ (see equation (11)) in log–log scale for a ER network with $\langle k \rangle = 4$ and $N = 10^5$ at $T = T_c = 0.25$. The symbols represent the simulation results obtained from 5000 stochastic realizations and the dashed line a power-law fit. The theoretical value of the exponent d_l is $d_l = 2$.

and the fraction of bridge nodes of the layer in which the disease originates, because when $t \leqslant t_b$ the disease has not reached the other layer.

Using the branching formalism (see appendix C) we obtain that at $T = T_c$, the average time at which the first bridge node is infected, is a decreasing function with the fraction r, as expected. Moreover, we obtain theoretically that the relation is a power law: $t_b \sim r^{-1/2}$ for homogeneous networks and $t_b \sim r^{-(\lambda-3)/(\lambda-2)}$ for SF networks with degree distribution $P(k) \sim k^{-\lambda}$ and $3 < \lambda < 4$ (see appendix C). In figure 2 we show the simulations and the theoretical solutions of t_b versus r at $T = T_c(r = 0)$ for these networks, and we obtain that the exponent is consistent with our theoretical predictions.

This relation between t_b and r can also be obtained using *scaling theory* [30]. Considering a Leath [31] or link percolation process at $T = T_c$, a finite cluster of occupied links leads to the set of recovered nodes in an outbreak which is originated from an index case. The size of this cluster is $\mathcal{R} \equiv R\,N$, where R is the fraction of recovered nodes and N is the size of the network. The average shortest path between all the nodes in that cluster is denoted by ℓ, which it is expected to be proportional to the duration of the outbreak. It is known that at criticality (i.e. at the critical point), $\mathcal{R} \sim \ell^{d_l}$, where d_l is the chemical dimension [32, 33]. We are interested in the time t_b that takes the disease to reach the first bridge node as a function of r (assuming that the cluster has at least one bridge node). Let us consider a finite cluster of size $\mathcal{R}$ with n bridge nodes, then we expect that if a node of the cluster is the index patient or the source of the epidemic, then the time t_b will be proportional to the distance between this index case and the nearest bridge node. The minimum chemical distance to the nearest bridge node can be found by partitioning the cluster into n subclusters, one for each bridge node (see figure 3(a)). Thus a node v in the cluster belongs to the subcluster of the bridge node u when the node u is the nearest bridge node of v among all the bridge nodes in the cluster. The average minimum chemical distance in each subcluster $\ell_{subcluster}$ behaves as ℓ since the cluster of infected nodes is a fractal at criticality [33]. Additionally, the average mass of each subcluster is $\mathcal{R}/n$ and at $T = T_c$ we expect that (see also, figure 3(b))

Figure 4. Time t_b as a function of r obtained from the equations of the appendix C. (a): for an ER network with $\langle k \rangle = 4$ for $T = 0.250\,625$ (black), $T = 0.250\,78$ (red), $T = 0.250\,976$ (green) and $T = 0.251\,220\,7$ (blue). (b): SF network with $k_{\min} = 2$ and $\lambda = 3.5$ for $T = 0.269\,325$ (black), $T = 0.269\,481$ (red), $T = 0.269\,92$ (green), and $T = 0.270\,226$ (blue). The main figures in panels (a) and (b) are in log-linear scale. The insets shows in log–log scale for identifying the slope of the logarithmic term in equation (14). The symbols are obtained from a logarithmic fit of the curves in the main plot for small values of r, and the dashed line is a power law fit. Panels (c) and (d) show the same curves as in (a) and (b), respectively, in log–log scale. The dashed lines are a power law fit with exponent -0.53 for the ER network and -0.35 for the SF network, which are consistent with the exponent $-1/d_l$ predicted in section 3.

$$\frac{\mathcal{R}}{n} \sim \ell_{\text{subcluster}}^{d_l}, \tag{11}$$

where $\ell_{\text{subcluster}}$ is the average shortest path from a node to the bridge node of this subcluster. Since the probability that a node is a bridge is uniform, the density of bridge nodes in the network is equal to the density of bridge nodes in the cluster of size $\mathcal{R}$, i.e. $n/\mathcal{R} \approx r$, which leads to
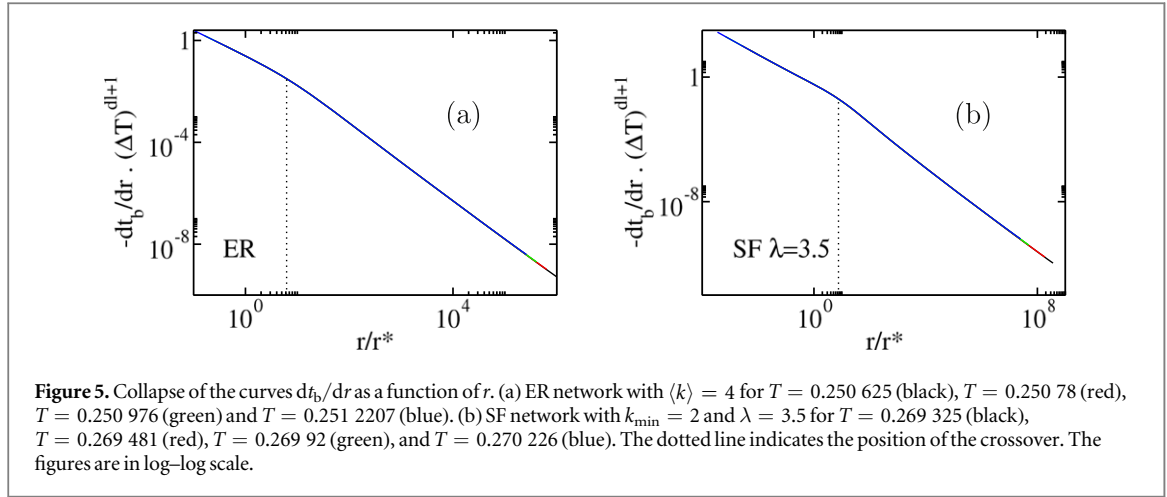
$$r^{-1} \sim \ell_{\text{subcluster}}^{d_l}. \tag{12}$$

On the other hand, we expect that $\ell_{\text{subcluster}} \sim t_b$ [34], so finally

$$t_b \sim r^{-1/d_l}. \tag{13}$$

For ER networks $d_l = 2$ and for SF networks with $3 < \lambda < 4$, $d_l = (\lambda - 2)/(\lambda - 3)$ [35].

4. Crossover regimes of t_b for $T \gtrsim T_c (r = 0)$

Integrating the equations of time evolution for the stochastic regime for $T \gtrsim T_c(r = 0)$ (see appendix C) we obtain that t_b as a function of r has two regimes, which are separated by a crossover at $r = r^*$ (see figures 4(a) and (b)). For $r > r^*$ we obtain that $t_b \sim r^{-1/d_l}$ as in the previous section. On the other hand, for $r < r^*$, the time t_b is a logarithmic function with r. This behavior is expected since for large r, the distance between the bridge nodes is small and the system is like at criticality. While for small values of r, the disease needs to cross longer distances to reach a bridge node and it behaves like above the criticality, i.e. the distance between two nodes is a logarithmic function of N [36]. Therefore, using similar arguments to the previous section, we can obtain the behavior $t_b \sim -\ln(r)$ for $r < r^*$. Indeed, from the numerical results we obtain that above criticality $t_b \sim A(T, T_c) - B \ln(r)$ for ER networks and SF networks with $3 < \lambda < 4$, i.e. the expected r dependence. In addition, we get that $A(T, T_c)$ is a function of the distance to the criticality $T - T_c$, and $B = (T - T_c)^{-1}$ for both topologies. Therefore, t_b behaves as

Figure 5. Collapse of the curves dt_b/dr as a function of r. (a) ER network with $\langle k \rangle = 4$ for $T = 0.250\,625$ (black), $T = 0.250\,78$ (red), $T = 0.250\,976$ (green) and $T = 0.251\,2207$ (blue). (b) SF network with $k_{min} = 2$ and $\lambda = 3.5$ for $T = 0.269\,325$ (black), $T = 0.269\,481$ (red), $T = 0.269\,92$ (green), and $T = 0.270\,226$ (blue). The dotted line indicates the position of the crossover. The figures are in log–log scale.

$$t_b \sim \begin{cases} A(T, T_c) - (T - T_c)^{-1}\ln(r) & \text{if } r \ll r^* \\ r^{-1/d_l} & \text{if } r \gg r^* \end{cases}. \tag{14}$$

The scaling results of equation (14) are supported by the numerical solution of the theory in the appendix C as seen in figure 4.

In the following, we study in more detail the transition between the logarithmic regime and the power-law regime.

In order to avoid to work with the y-intercept (i.e. the function $A(T, T_c)$) and the logarithmic function, instead of using the equation (14), we will work with the derivative of t_b with respect to r.

Based on equation (14) we propose the following scaling Anzat for dt_b/dr,

$$\frac{dt_b}{dr} \sim \begin{cases} -(\Delta T)^{-1}\dfrac{1}{r}; & \text{if } r < r^* \\ -\dfrac{1}{d_l}r^{-(1/d_l+1)} & \text{if } r > r^* \end{cases}. \tag{15}$$

The crossover is defined by the point $r = r^*$ at which both regimes intersects, and is given by

$$r^* \sim (\Delta T)^{d_l}. \tag{16}$$

In addition, we have that at $r = r^*$,

$$\left.\frac{dt_b}{dr}\right|_{r=r^*} \sim \Delta T^{-(d_l+1)}. \tag{17}$$

Applying to the function dt_b/dr the transformations: $r \to r/r^*$ and $dt_b/dr \to dt_b/dr\,\Delta T^{d_l+1}$ (where $\Delta T \equiv T - T_c$) we obtain that the curves dt_b/dr collapse (see figure 5). Therefore, equation (15) can be written as

$$\frac{dt_b}{dr} = \Delta T^{-(d_l+1)}F\left(\frac{r}{r^*}\right), \tag{18}$$

where $F(x)$ is given by

$$F(x) \sim \begin{cases} x^{-1}; & \text{if } x \ll 1 \\ x^{-(d_l+1)/d_l} & \text{if } x \gg 1 \end{cases} \tag{19}$$
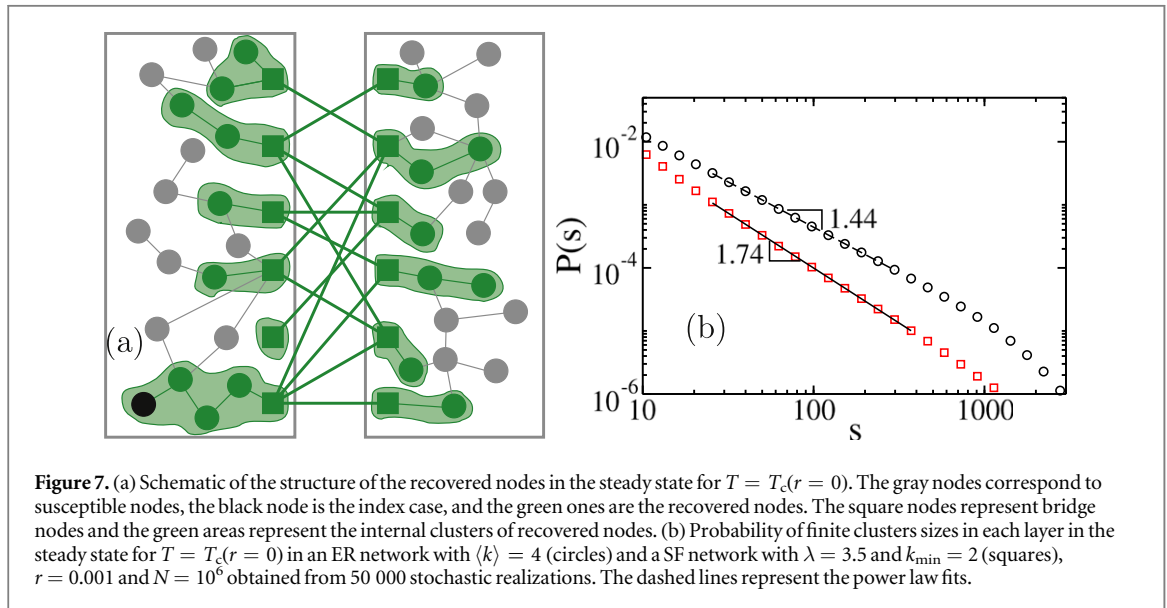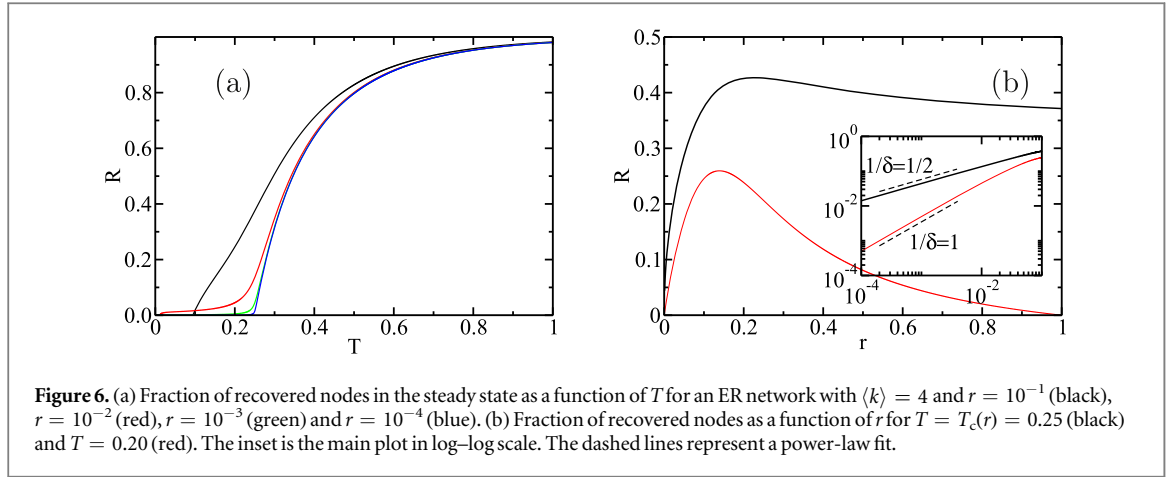
with $x = r/r^*$.

Besides the rich behavior of t_b which corresponds to the beginning of the epidemic, in the next section we will show that in the steady state, the bridge nodes also generates a power-law behavior in the fraction of recovered nodes as a function of r, similar to Dong *et al* [11]. However, unlike [11] which interpreted that power-law as an external field, we will explain this behavior from a geometrical point of view.

5. The steady state

5.1. $T \leqslant T_c$

In our model with two layers, increasing fraction of bridge nodes generates a large number of infected nodes since bridge nodes have a high external degree. However, an increase in r decreases the external connectivity

Figure 6. (a) Fraction of recovered nodes in the steady state as a function of T for an ER network with $\langle k \rangle = 4$ and $r = 10^{-1}$ (black), $r = 10^{-2}$ (red), $r = 10^{-3}$ (green) and $r = 10^{-4}$ (blue). (b) Fraction of recovered nodes as a function of r for $T = T_c(r) = 0.25$ (black) and $T = 0.20$ (red). The inset is the main plot in log–log scale. The dashed lines represent a power-law fit.

Figure 7. (a) Schematic of the structure of the recovered nodes in the steady state for $T = T_c(r = 0)$. The gray nodes correspond to susceptible nodes, the black node is the index case, and the green ones are the recovered nodes. The square nodes represent bridge nodes and the green areas represent the internal clusters of recovered nodes. (b) Probability of finite clusters sizes in each layer in the steady state for $T = T_c(r = 0)$ in an ER network with $\langle k \rangle = 4$ (circles) and a SF network with $\lambda = 3.5$ and $k_{\min} = 2$ (squares), $r = 0.001$ and $N = 10^6$ obtained from 50 000 stochastic realizations. The dashed lines represent the power law fits.

which reduces the disease propagation. Therefore, there exist a nonlinear relation between R and r, as can be seen in figure 6. In the appendix A we show that this behavior does not depend on the value of $\langle k_{\text{ext}} \rangle r$. In addition, for $r \to 0$, we observe (see inset of figure 6(b)) that R as a function of r is a power-law with exponent $1/\delta = 1/2$ for $T = T_c(r = 0)$ and $1/\delta = 1$ for $T < T_c(r = 0)$.

The origin of the exponent at $T = T_c(r = 0)$ is due to the particular structure of the cluster of recovered nodes since the infection tree is composed by finite clusters of recovered nodes in each layer, that are connected through bridge nodes (see figure 7(a)). In figure 7(b) we show the probability of recovered clusters $P(s)$ of size s in each layer (obtained from stochastic simulations in a ER network and SF network with $\lambda = 3.5$ at $T = T_c(r = 0)$) which follows a power-law distribution with exponent $\tau - 1$, where $\tau = 5/2$ for ER networks and $\tau = 2 + 1/(\lambda - 2) = 2.66$ for SF networks with $\lambda = 3.5$ [37].

In the following, we present a geometric interpretation of our model and show theoretically that the structure of the infection tree explains the exponent of the power-law between R and r, using the probability $P(s)$.

In our model it is expected that as $r \to 0$ at $T = T_c(r = 0)$, almost every bridge nodes will be infected since they have a large external connectivity. Each of these nodes will be the seed of the finite outbreak or cluster in each layer. In this case, the infection tree is composed by these finite clusters and hence the fraction of recovered nodes is proportional to the sum of the sizes of these finite clusters in which one node of each cluster is a bridge node. This can be written as

$$
\begin{aligned}
R = {} & P(s = 1)(1 - (1 - r)^1)x + P(s = 2)(1 - (1 - r)^2)x^2 \\
& + P(s = 3)(1 - (1 - r)^3)x^3 + ...,
\end{aligned}
\tag{20}
$$

where $P(s)$ is the probability that a randomly chosen node belongs to a cluster of size s and $(1 - (1 - r)^s)$ is the probability that this cluster has a bridge node (with $x = 1$). We can approximate R as

$$R = 1 - \sum_{i=1}^{\infty} P(s)(1-r)^i \tag{21}$$

$$\approx 1 - A \int_1^{\infty} P(s)(1-r)^s \mathrm{d}s \tag{22}$$

$$\approx 1 - A \int_1^{\infty} P(s)\exp(s\ln(1-r))\mathrm{d}s. \tag{23}$$

If $r \ll 1$ then $\exp(s\ln(1-r)) = (1-r)^s \approx 1 - rs$, and when $T < T_c$ it holds that $P(s) \sim s^{-\tau+1}\exp(-s/s_{\max})$ [38], where $s_{\max} \sim |T - T_c|^{-1/\sigma}$. Thus,

$$R \approx 1 - A \int_1^{\infty} (1-rs)s^{-\tau+1}\exp(-s/s_{\max})\mathrm{d}s, \tag{24}$$

where

$$A = \frac{1}{\int_1^{\infty} s^{-\tau+1}\exp(-s/s_{\max})\mathrm{d}s}. \tag{25}$$

Since for $T < T_c$, $\int_1^{\infty} s^{-\tau+2}\exp(-s/s_{\max})\mathrm{d}s$ does not diverge when $r \to 0$, then we obtain that, $R \sim r$, i.e.

$$1/\delta = 1, \tag{26}$$

for $T < T_c$.

On the other hand, for $T = T_c$, $s_{\max} \to \infty$; and if $r \ll 1$ then $\ln(1-r) \approx -r$. In this case R can be approximated by[6]

$$\approx 1 - A \int_1^{\infty} s^{-\tau+1}\exp(-rs)\mathrm{d}s, \tag{27}$$

with

$$A = \frac{1}{\int_1^{\infty} s^{-\tau+1}\mathrm{d}s} = -\tau + 2. \tag{28}$$

Denoting $u = rs$, and integrating by part

$$\approx 1 - \frac{-\tau+2}{r^{-\tau+2}} \int_r^{\infty} u^{-\tau+1}\exp(-u)\mathrm{d}u$$

$$\approx 1 - \frac{-\tau+2}{r^{-\tau+2}} \left(\frac{1}{-\tau+2}r^{-\tau+2} - \int_r^{\infty} u^{-\tau+2}\exp(-u)\mathrm{d}u \right)$$

$$\approx \frac{-\tau+2}{r^{-\tau+2}} \int_r^{\infty} u^{-\tau+2}\exp(-u)\mathrm{d}u \sim r^{\tau-2}, \tag{29}$$

so finally, $R \sim r^{\tau-2}$, i.e.

$$1/\delta = \tau - 2. \tag{30}$$

Thus, for $T = T_c$, the exponent of the scaling relation between R and r is related to the Fisher exponent of the finite size cluster distribution. Therefore at criticality, alternatively to the interpretation of the exponent $1/\delta$ as the result of an 'external field' [11], here we show theoretically that this exponent can be understood from the distribution of finite cluster sizes in one layer. This exponent was also studied in the context of semiconductors and percolation in the presence of a 'ghost field' [30, 39, 40].

5.2. $T > T_c$

While above criticality, R does not go to zero when $r \to 0$, we obtain theoretically that $\frac{\mathrm{d}R}{\mathrm{d}r}|_{r\to 0} \sim (\Delta T)^{-1}$ for ER and SF networks. Here, $\frac{\mathrm{d}R}{\mathrm{d}r}|_{r\to 0}$ is related to the divergence of the average size of the finite clusters (see appendix B).

On the other hand, above criticality the contribution of finite clusters to the GC is dependent on two factors. First, note that in equation (27) the contribution of the finite size cluster distribution $P(s)$ that compose the GC is constrained by an exponential function $\exp(-s/s_r) = \exp(-rs)$, where $s_r = 1/r$ is the cutoff imposed by the fraction of bridge nodes. This is due to the fact that during the dynamic process, the finite clusters cannot grow without any constrain because these clusters interfere with each other. Second, for single networks, it is known that above criticality, $P(s) \sim s^{-\tau}\exp(-s/s_{\max})$ where $s_{\max} \sim |T - T_c|^{-1/\sigma}$, i.e. there is another cutoff imposed by the transmissibility. Therefore in a bilayer network for $T > T_c$, the cutoff of the finite size distribution in one layer can be imposed either by the fraction of bridge nodes or by the transmissibility. When the transmissibility is

---

[6] Note that we do not use the approximation $(1-r)^s \approx 1 - rs$ because it would lead to a divergent integral.

very close to T_c or r is not small, then $s_r \ll s_{\max}$ i.e. the cutoff imposed by the bridge nodes dominates the finite cluster distribution, and the system behaves as at criticality, since it does not 'see' the cutoff imposed by the transmissibility. The opposite occurs when T is well above T_c or $r \ll 1$. Denoting $r^\dagger$ as the value of the fraction of bridge nodes at which both cutoffs are comparable, then

$$r^\dagger \sim |T - T_c|^{1/\sigma}, \tag{31}$$

and using that $\sigma = 1/(d_l \nu_l)$ [35], we obtain that

$$r^\dagger \sim (|T - T_c|^{\nu_l})^{d_l}, \tag{32}$$

Finally, since for uncorrelated homogeneous networks and SF networks $\nu_l = 1$ [35],

$$r^\dagger \sim |T - T_c|^{d_l}, \tag{33}$$

which is the same relation as in equation (16), i.e. the crossover r^* of the time t_b between the logarithmic regime and the power law regime. Thus, the crossover of the time t_b scales with $T - T_c$ as the crossover $r^\dagger$ between the cutoff imposed by the transmissibility and the cutoff imposed by the bridge nodes. Therefore $r^\dagger \sim r^*$. Moreover, since the correlation length behaves as $\xi \sim |T - T_c|^{-\nu_l}$ (where $\nu_l = 1$ for ER and SF networks, as mentioned above), this result suggests that the coefficient of the logarithmic term in equation (14) is related to the correlation length.

6. Real networks

We next examine how the topology and the selection of bridge nodes (targeted or random) affects t_b.

Flight transportation data are widely available through different online sources. In this work, we considered the Flightradar24 flight tracker [41] as the main source of data in order to demonstrate our results on a real world example of a two layer complex network. In this work, we consider our flight networks as being the networks where the airports are represented by nodes and the routes among them by links. According to its own website description, Flightradar24 is a flight tracker that shows live air traffic from around the world. Flightradar24 combines data from several data sources including automatic dependent surveillance-broadcast (ADS-B), Multilateration (MLAT) and radar data. The ADS-B, MLAT and radar data is aggregated together with schedule and flight status data from airlines and airports to create their flight tracker datasets with live online access. For security and privacy reasons information about some aircraft is limited or blocked. This includes most military aircraft and certain high profile aircraft. The site provides information of current and historical flights, such as the destination and origin airports, the flight status (flight codes, arrival and departures times, etc), airlines and aircraft models. For the purpose of this work, we build two different networks. One considering only those flights within the United States, another within Europe, both connected by links represented by the flights among them (between bridge nodes). It was shown that these flights networks typically have a highly connected set of core airports (mainly hubs) and a few connections to and among periphery airports, in a so called core-periphery structure, typical for real-world airline networks [42]. In figure 8 we show both networks and their actual degree distribution $P(k)$.

Since these networks have a finite size, we use the effective critical transmissibility which is obtained by measuring the position of the peak of the second largest cluster size in a link percolation process as a function of the link occupation probability. In figure 9 we plot t_b as a function of r for $T = T_c$ of each network in the main figure and for $T \geqslant T_c$ in the insets obtained from the simulations. In these subfigures we find that when $T > T_c$ the time t_b behaves as a logarithmic function with r. However, for $T = T_c$ we cannot observe a power law behavior as predicted by our theory in section 4 due to finite size effects ($N \sim 10^3$). On the other hand, from the main figures, we can see that the real network with the real bridge nodes has a smaller t_b than expected for randomly chosen bridge nodes. This is due to the fact that the actual bridge nodes have an average degree well above $\langle k \rangle$. Specifically, $\langle k \rangle = 26.5$ for Europe and $\langle k \rangle = 17.9$ for USA, while the average connectivities of the actual bridge nodes are: 77.3 and 90.2, respectively. Since these bridges airports have a higher degree than the average $\langle k \rangle$, then they can be infected more quickly than other airports. To test this effect of the degree of the bridge nodes on t_b, we analyze in figure 9 the time t_b as a function r, in which the fraction r corresponds to the nodes with the highest degree, called 'targeted bridge nodes'. Indeed, we obtain that the disease reaches a bridge node earlier that in the case of randomly chosen bridge nodes. Furthermore, the time t_b for the targeted case is in agreement with the case for the actual fraction of bridge nodes (see the green cross in figure 9).

On the other hand, to study the effect of the topology on t_b in real finite networks, we also compute t_b versus r for an infinite synthetic uncorrelated network with the actual degree distribution as a 'null model' (i.e. as a baseline to compare with the real network), using the equations of the appendix C. For randomly chosen bridge nodes, we obtain that for small values of r a finite network has a smaller time t_b than an infinite network, which is expected since the loops or cycles in a finite network would tend to decrease the distance between nodes and

Figure 8. Real airline networks and their degree distribution for Europe (a) and USA (b), obtained from the Flightradar24 data [41]. The sizes are: $N = 425$ for Europe and $N = 973$ for USA, and the number of links are: 5636 and 8724, respectively. The degree–degree (r_p) correlation and clustering coefficients (C) are: $r_p = -0.14$ and $C = 0.59$ for Europe, and $r_p = 0.09$ and $C = 0.30$ for USA.

Figure 9. (a) t_b versus r for Europe with $T_c = 0.019$ and (b) USA with $T_c = 0.021$. The solid black line is obtained from the equations derived in appendix C using the real degree distribution, and choosing randomly the bridge nodes. The red and blue symbols correspond to the real networks with random and targeted bridge nodes, respectively. Finally the green symbol is obtained from the real network and the real bridge nodes (fixed r value). In the insets we show t_b versus r for the real networks with randomly chosen bridge nodes, in linear-log scale for (from up to down): $T = T_c$, $T = 0.05$, $T = 0.10$, $T = 0.15$ and $T = 0.20$. We average our simulation results over 10^4 stochastic realizations.

hence the time to reach a bridge node. Notably, for larger values of r, t_b versus r is almost the same for an infinite uncorrelated network and a finite real networks. This result indicates that in this regime the topology magnitudes like the degree–degree correlation and clustering are less important to predict t_b. Indeed, as $r \to 1$, the probability that the first infected node is a bridge, increases. Therefore, the effect of the core-periphery structure, clustering and degree–degree correlation on t_b should not affect the value of t_b.

7. Conclusions

Since in real networks, like in the flight network, the bridge nodes are vulnerable and are able to boost the spreading of a disease, it is important to understand their role in the spreading. In this paper, we study the effect

of the bridge nodes on the dynamic spreading in a two layer network. We obtain that at criticality, these nodes are crucial for spreading the disease to the entire global system and their presence induces a double peak on the number of infected individuals during the dynamic which corresponds to the infection of the bridge and non-bridge nodes. Moreover, the fraction of infected nodes increases rapidly after the disease reaches the first bridge node, so the time t_b at which the epidemic reaches this node is of great importance to predict the 'explosion' of the epidemic. We showed that at criticality in the stochastic regime of the spreading process the time t_b behaves as a power law with the fraction of bridge nodes r, with an exponent related to the chemical dimension. Additionally, above criticality, t_b follows a scaling function with two regimes separated by a crossover $r = r^*$. For $r < r^*$ t_b behaves a logarithmic function while for $r > r^*$, it follows a power-law function. We showed that this behavior emerges as the result of the 'competition' between two scales: one imposed by the transmissibility through the correlation length and the other imposed by the fraction of bridge nodes which constrain the size of a finite infected cluster. On the other hand, in the steady state, we showed that at criticality the fraction of recovered nodes obeys a power law function with r. We find that the origin of the exponent is related to the finite cluster size distribution since the structure of the epidemic cluster is composed by a distribution of finite clusters in each layer which are connected by the bridge nodes. Finally, we applied our model on real flight networks and obtained that a targeted fraction of bridge nodes reduces the time t_b, and as r increases, the structure of the network becomes less relevant to predict the value of t_b.

The model and results presented in this paper could be generalized. For example, our model could be extended to more layers and other epidemic models like the susceptible-infected-susceptible model, in order to evaluate the role of the bridge nodes in more complex structures and different dynamic processes. In addition, different effective control methods could be studied with the goal of increasing the time t_b in real-world networks.

Acknowledgments

Appendix A. R versus r

In figure A1 we show the relation between R and r for different number of external links, i.e $\langle k_{\text{ext}} \rangle r = c$ (see section 2).

Appendix B. Scaling of dR/dr for $T \gtrsim T_c$

In this section we will obtain the scaling relation between dR/dr and the distance to criticality $T - T_c$ in the limit of $r \rightarrow 0$, i.e. $dR/dr \sim (T - T_c)^{-\gamma}$ where γ is the critical exponent of the mean size of finite clusters. We apply our equations for homogeneous networks and SF networks with $3 < \lambda < 4$. Note that in our calculation the external connectivity distribution always follows a Poisson distribution with $\langle k_{\text{ext}} \rangle \sim 1/r$.

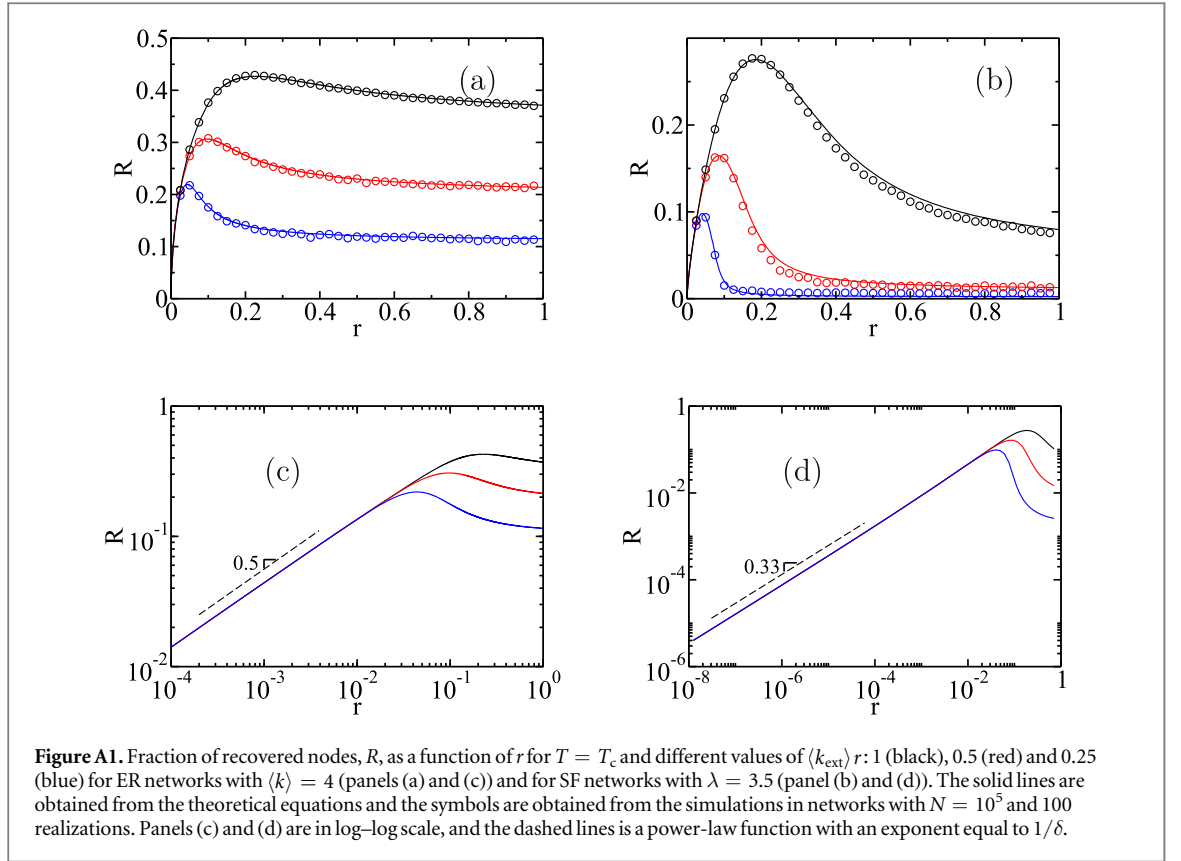For any value of r, the fraction of nodes that belong to the GC R is given by

$$R = 1 - [(1 - r)G_0^i(1 - Tf_\infty^i) + rG_0^i(1 - Tf_\infty^i)G_0^b(1 - Tf_\infty^b)], \tag{B.1}$$

where f_∞^i and f_∞^b satisfy the following equations,

$$f_\infty^i = 1 - [(1 - r)G_1^i(1 - Tf_\infty^i) + rG_1^i(1 - Tf_\infty^i)G_0^b(1 - Tf_\infty^b)], \tag{B.2}$$

$$f_\infty^b = 1 - G_1^b(1 - Tf_\infty^b)G_0^i(1 - Tf_\infty^i), \tag{B.3}$$

In the limit of $r \rightarrow 0$, $\langle k_{\text{ext}} \rangle \rightarrow \infty$ and since $G_0^b(x) = G_1^i(x) = \exp(\langle k_{\text{ext}} \rangle (x - 1))$, then for any value of $x < 1$, it is straightforward that $G_0^b(x) = G_1^i(x) \rightarrow 0$. Therefore in this limit the fraction of nodes in the GC can be approximated by,

Figure A1. Fraction of recovered nodes, R, as a function of r for $T = T_c$ and different values of $\langle k_{ext} \rangle r$: 1 (black), 0.5 (red) and 0.25 (blue) for ER networks with $\langle k \rangle = 4$ (panels (a) and (c)) and for SF networks with $\lambda = 3.5$ (panel (b) and (d)). The solid lines are obtained from the theoretical equations and the symbols are obtained from the simulations in networks with $N = 10^5$ and 100 realizations. Panels (c) and (d) are in log–log scale, and the dashed lines is a power-law function with an exponent equal to $1/\delta$.

$$R = 1 - [(1 - r)G_0^i(1 - Tf_\infty^i)], \tag{B.4}$$

with

$$f_\infty^i = 1 - [(1 - r)G_1^i(1 - Tf_\infty^i)]. \tag{B.5}$$

Note that equation (B.5) is the same as in a single network with a perturbation r. Additionally in this limit, equation (B.3) reduces to $f_\infty^b = 1$, i.e. the probability that an external link leads to a bridge node that belong to the GC is equal to one because these nodes have an increasing number of external links ($\langle k_{ext} \rangle \rightarrow \infty$). Since these equations depend only in variables related to the internal links, for simplicity we will omit the index i.

Taking the derivative of the equations (B.4) and (B.5) with respect to r, we obtain for $r \rightarrow 0$:

$$\frac{dR}{dr}\bigg|_{r=0} = G_0(1 - Tf_\infty) + TG_0'(1 - Tf_\infty)\frac{df_\infty}{dr}\bigg|_{r=0}, \tag{B.6}$$

$$\frac{df_\infty}{dr}\bigg|_{r=0} = \frac{G_1(1 - Tf_\infty)}{1 - TG_1'(1 - Tf_\infty)}. \tag{B.7}$$

In the following, we will apply these equations for homogeneous and SF networks with $3 < \lambda < 4$.

B.1. Homogeneous networks

For the case of homogeneous networks, i.e. with finite third-order moment, we can expand the self-consistent equation (B.5) around $f_\infty = 0$ up to the quadratic term for T near T_c, obtaining

$$f_\infty = \frac{2G_1'(1)}{T^2G_1''(1)}(T - T_c). \tag{B.8}$$

Similarly, expanding $G_1'(1 - Tf_\infty)$ and $G_1(1 - Tf_\infty)$ in equation (B.7), we obtain

$$\frac{df_\infty}{dr}\bigg|_{r=0} = \frac{1 - TG_1'(1)f_\infty}{1 - T(G_1'(1) - TG_1''(1)f_\infty)}. \tag{B.9}$$

Then, using equation (B.8), the derivative of f_∞ with respect to r when $r \rightarrow 0$ behaves as

$$\frac{df_\infty}{dr}\bigg|_{r=0} \approx \frac{1}{G_1'(1)(T - T_c)}. \tag{B.10}$$

Finally, expanding $G_0'(1 - Tf_\infty)$ in equation (B.6) around $f_\infty = 0$ up to the linear term and using that $T_c = G_0'(1)/G_0''(1)$, leads to

$$\left.\frac{dR}{dr}\right|_{r=0} = G_0(1 - Tf_\infty) + G_0'(1)\left(1 - \frac{T}{T_c}f_\infty\right)T\left.\frac{df_\infty}{dr}\right|_{r=0}, \tag{B.11}$$

and replacing equation (B.10) in the last expression, we obtain

$$\left.\frac{dR}{dr}\right|_{r=0} = G_0(1 - Tf_\infty) + \frac{T_c}{T - T_c}\frac{G_0'(1)}{G_1'(1)}. \tag{B.12}$$

Since in the last equation, as $T \to T_c$, the first term is finite while the second one diverges, we disregard the first term and the derivative of R with r, is given by,

$$\left.\frac{dR}{dr}\right|_{r=0} \approx \frac{T_c}{T - T_c}\frac{G_0'(1)}{G_1'(1)} \sim (T - T_c)^{-1}, \tag{B.13}$$

i.e. $\gamma = 1$ for homogeneous networks.

B.2. SF networks with $3 < \lambda < 4$

For the case of SF networks with $3 < \lambda < 4$ and using Tauberian theorems [43], the expansion of equation (B.5) around $f_\infty = 0$ is

$$f_\infty = 1 - (1 - G_1'(1)Tf_\infty + c_1 f_\infty^{\lambda-2}), \tag{B.14}$$

where c_1 is a constant. This expression leads to

$$f_\infty \sim (T - T_c)^{1/(\lambda-3)}. \tag{B.15}$$

Similarly, expanding $G_1(1 - Tf_\infty)$ and $G_1(1 - Tf_\infty)$ in equation (B.7), we obtain

$$\left.\frac{df_\infty}{dr}\right|_{r=0} \approx \frac{1 - G_1'(1)Tf_\infty + c_1 f_\infty^{\lambda-2}}{1 - T(G_1'(1) - c_2 Tf_\infty^{\lambda-3})}, \tag{B.16}$$

where c_1 and c_2 are constants. Using that $T_c = 1/G_1'(1)$, and the equation (B.15), the last equation can be approximated by,

$$\left.\frac{df_\infty}{dr}\right|_{r=0} \approx \frac{1 - G_1'(1)Tc_3 (T - Tc)^{1/(\lambda-3)} + c_4 (T - Tc)^{(\lambda-2)/(\lambda-3)}}{c_5(T - Tc)}, \tag{B.17}$$

where c_3, c_4, c_5 are constants.

Since $\lambda > 3$ then for $T \to T_c$, in the numerator of the last equation only the first term remains, and hence

$$\left.\frac{df_\infty}{dr}\right|_{r=0} \approx \frac{1}{c_5(T - Tc)} \sim (T - T_c)^{-1}. \tag{B.18}$$

On the other hand, applying Tauberian theorems [43], and inserting equations (B.15) and (B.18) into equation (B.6), leads to the following relation

$$\left.\frac{dR}{dr}\right|_{r=0} \approx G_0(1 - Tf_\infty) + (G_0'(1) - G_0''(1)Tf_\infty)$$
$$+ c_6 (T - T_c)^{(\lambda-2)/(\lambda-3)}\frac{c_7 T}{T - T_c}. \tag{B.19}$$

In the limit $T \to T_c$, the first term is finite while the second one diverges, hence the first term can be disregarded. In turn, the numerator of the second term is also finite, which finally leads to
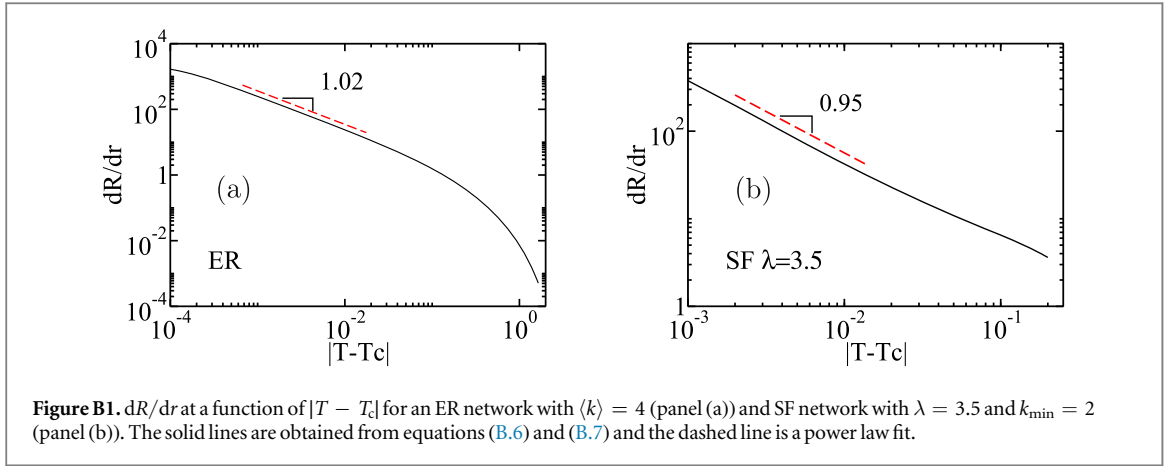
$$\left.\frac{dR}{dr}\right|_{r=0} \sim (T - T_c)^{-1}. \tag{B.20}$$

i.e. $\gamma = 1$.

In figure B1 we show dR/dr as a function of $|T - T_c|$ for an ER network and a SF network with $\lambda = 3.5$, in which we can observe that the exponent obtained is consistent with the predicted value.

Appendix C. Mean time t_b to reach a bridge node

In order to compute the time it takes the disease to reach a bridge node, we describe the disease spreading with $t_r = 1$ as a branching process.

Figure B1. dR/dr at a function of $|T - T_c|$ for an ER network with $\langle k \rangle = 4$ (panel (a)) and SF network with $\lambda = 3.5$ and $k_{\min} = 2$ (panel (b)). The solid lines are obtained from equations (B.6) and (B.7) and the dashed line is a power law fit.

Let us consider an infected individual in generation n, then the generating function of the probability to not reach a bridge node in the following generation through a link is given by

$$G_{1b}(x) \equiv 1 - T + T(1 - r) G_1(x), \tag{C.1}$$

where T is the transmissibility and $G_1(x)$ is the generating function of the excess degree distribution. Similarly the generating function of the probability to not reach a bridge node in the following n-generations through a link is given by

$$g_n(x) \equiv \underbrace{G_{1b}(G_{1b}(\cdots G_{1b}(x)))}_{(n)}, \tag{C.2}$$

for $n \geqslant 1$, and $g_0(x) = x$ for $n = 0$. On the other hand, the generating function of the probability to not reach a bridge node in the following n-generations from the index case is $G_0(g_n(x))$, where $G_0(x)$ is the generating function of the degree distribution. Therefore, the probability that in generation $n + 1$ the disease reaches a bridge node is,

$$
\begin{aligned}
P(t = n + 1) &= (1 - r)[G_0(g_n(1)) - G_0(g_n(1 - Tr))] \\
&= (1 - r)[G_0(g_n(1)) - G_0(g_{n+1}(1))], \tag{C.3}
\end{aligned}
$$

where $G_0(g_n(1))$ is the probability that the disease reaches the generation $n + 1$, i.e. is the probability that there is an infected node in generation $n + 1$, and $G_0(g_n(1 - Tr))$ is the probability to not reach a bridge node in generation $n + 1$. For $n = 0$ we set $P(t = 0) = r$.

Since, we only consider those realizations in which one of the infected node is a bridge, we normalize the probability $P(t = n)$:

$$Q(t = n) \equiv \frac{P(t = n)}{\sum_{i=0}^{\infty} P(t = i)}. \tag{C.4}$$

Finally, the average time t_b to reach a bridge node is given by

$$t_b = \sum_{n=0}^{\infty} n Q(t = n). \tag{C.5}$$

C.1. Scaling relation between t_b and r at $T = T_c$

In the following we will study the asymptotic behavior of $P(t = n)$ for large values of n and $r \ll 1$ at $T = T_c$.

Since g_n is the recursive iteration of the function $G_{1b}(x)$, the value of g_n tends to the solution of

$$x = G_{1b}(x), \tag{C.6}$$

as in a fixed point iteration process. We denote as g_∞ the solution of this equation. Therefore, for large values of n we can approximate equation (C.3) to

$$P(t = n + 1) \approx G_0'(g_\infty)(g_n - g_{n+1}). \tag{C.7}$$

Since $g_n = G_{1b}(g_{n-1})$, $g_{n+1} = G_{1b}(g_n)$ and $g_n \approx g_{n+1} \approx g_\infty$ we can approximate the last equation to

$$P(t = n + 1) \approx G_0'(g_\infty) G_{1b}'(g_\infty)(g_{n-1} - g_n). \tag{C.8}$$

If we use the approximation $g_{n-1} - g_n \approx G_{1b}'(g_\infty)(g_{n-2} - g_{n-1})$ then equation (C.8), can be rewritten as

$$P(t = n + 1) \approx G_0'(g_\infty) G_{1b}'(g_\infty) G_{1b}'(g_\infty)(g_{n-2} - g_{n-1}), \tag{C.9}$$

and using equation (C.8) at $t = n - 1$ we obtain that

$$P(t = n + 1) \approx G'_{1b}(g_\infty)P(t = n). \tag{C.10}$$

This relation shows that for large values of n, the distribution $P(t)$ corresponds to an exponential distribution with a mean time value of $t_b = 1/(\ln(G'_{1b}(g_\infty)))$. Since for $r \to 0$ and $T = T_c$, we have that $g_\infty \to 1$ and $G'_{1b}(g_\infty) \to 1$, then $\ln(G'_{1b}(g_\infty)) \approx 1 - G'_{1b}(g_\infty)$, i.e.

$$t_b \approx \frac{1}{1 - G'_{1b}(g_\infty)}. \tag{C.11}$$

In the following we will explore the relation between $G'_{1b}(g_\infty)$ and r for homogeneous networks, i.e. with finite third order moment in the degree distribution, and SF networks with $3 < \lambda < 4$.

C.1.1. Homogeneous networks. As $r \to 0$, the solution g_∞ tends to the value $g_\infty = 1$. Therefore, expanding equation (C.6) around this value we have that

$$
\begin{aligned}
g_\infty &= 1 - T_c + T_c(1 - r)\left(1 + G_1'(1)(g_\infty - 1) + \frac{1}{2}G_1''(1)(g_\infty - 1)^2\right), \\
&= 1 - T_c + T_c(1 - r) + (1 - r)(g_\infty - 1) \\
&\quad + T_c(1 - r)\frac{1}{2}G_1''(1)(g_\infty - 1)^2,
\end{aligned}
\tag{C.12}
$$

in which the physical solution of this equation is

$$g_\infty = 1 + \frac{r - r^{1/2}\sqrt{r + 2(1 - r)T_c^2 G_1''(1)}}{T_c(1 - r)G_1''(1)}. \tag{C.13}$$

In the limit of $r \to 0$ we have g_∞ behaves as

$$g_\infty = 1 - \sqrt{\frac{2}{G_1''(1)}}\, r^{1/2}. \tag{C.14}$$

Since $g_\infty \approx 1$, we can approximate $G'_{1b}(g_\infty)$ by

$$
\begin{aligned}
G_{1b}'(g_\infty) &\approx T_c(1 - r)(G_1'(1) + G_1''(1)(g_\infty - 1) + \cdots), \\
&\approx 1 - T_c\sqrt{2G_1''(1)}\, r^{1/2}.
\end{aligned}
\tag{C.15}
$$

Therefore, according to equation (C.11) the mean time t_b scales with r as,

$$t_b \sim r^{-1/2}, \tag{C.16}$$

for homogeneous networks, i.e. with a finite third order moment of the degree distribution.

C.1.2. SF networks with $3 < \lambda < 4$. Similarly, for SF networks with $3 < \lambda < 4$ and using Tauberian theorems [43], the expansion of equation (C.11) is given by

$$g_\infty = 1 - T_c + T_c(1 - r)(1 - G_1'(1)(1 - g_\infty) + c_0(1 - g_\infty)^{\lambda - 2}), \tag{C.17}$$

where c_0 is a constant. In the limit $r \to 0$, $g_\infty \to 1$, and hence $(1 - g_\infty) \ll T_c$. Therefore, the solution of equation (C.17) is

$$g_\infty \approx 1 - c_1 r^{\frac{1}{\lambda - 2}}, \tag{C.18}$$

where c_1 is a constant.

In order to find the value of t_b, we have to insert this solution in equation (C.11). Note that for SF networks with $3 < \lambda < 4$ the following relation holds,

$$G_1'(x) \approx G_1'(1) - c_2(1 - x)^{\lambda - 3}. \tag{C.19}$$

Therefore, the expansion of $G_{1b}(x)$ around $x = 1$ is

$$G_{1b}'(x) \approx T_c(1 - r)(G_1'(1) - c_2(1 - x)^{\lambda - 3}), \tag{C.20}$$

$$\approx (1 - r) - c_3(1 - x)^{\lambda - 3}, \tag{C.21}$$

where c_2 and c_3 are constants. For $x = g_\infty$, $r \ll 1$ and using the equation (C.18) we obtain,

$$G_{1b}'(g_\infty) \sim 1 - c_4 r^{\frac{\lambda - 3}{\lambda - 2}}. \tag{C.22}$$

Thus, the mean time t_b for SF networks with $3 < \lambda < 4$ is

$$t_b \sim r^{-\frac{\lambda-3}{\lambda-2}}. \tag{C.23}$$

References

[1] Brankston G, Gitterman L, Hirji Z, Lemieux C and Gardam M 2007 Transmission of influenza A in human beings *Lancet Infect. Dis.* **7** 257–65

[2] Faye O *et al* 2015 Chains of transmission and control of ebola virus disease in Conakry, Guinea, in 2014: an observational study *Lancet Infect. Dis.* **15** 320–6

[3] Rothenberg R B, Sterk C, Toomey K E, Potterat J J, Johnson D, Schrader M and Hatch S 1998 Using social network and ethnographic tools to evaluate syphilis transmission *Sex. Transm. Infect.* **25** 154–60

[4] Pastor-Satorras R, Castellano C, Van Mieghem P and Vespignani A 2015 Epidemic processes in complex networks *Rev. Mod. Phys.* **87** 925

[5] Wang Z, Bauch C T, Bhattacharyya S, d'Onofrio A, Manfredi P, Perc M, Perra N, Salathé M and Zhao D 2016 Statistical physics of vaccination *Phys. Rep.* **664** 1–113

[6] Buldyrev S V, Parshani R, Paul G, Stanley H E and Havlin S 2010 Catastrophic cascade of failures in interdependent networks *Nature* **464** 1025

[7] Shu P, Tang M, Gong K and Liu Y 2012 Effects of weak ties on epidemic predictability on community networks *Chaos* **22** 043124

[8] Newman M E, Strogatz S H and Watts D J 2001 Random graphs with arbitrary degree distributions and their applications *Phys. Rev.* E **64** 026118

[9] Kivelä M, Arenas A, Barthelemy M, Gleeson J P, Moreno Y and Porter M A 2014 Multilayer networks *J. Complex Netw.* **2** 203–71

[10] De Domenico M, Granell C, Porter M A and Arenas A 2016 The physics of spreading processes in multilayer networks *Nat. Phys.* **12** 901

[11] Dong G, Fan J, Shekhtman L M, Shai S, Du R, Tian L, Chen X, Stanley H E and Havlin S 2018 Resilience of networks with community structure behaves as if under an external field *Proc. Natl Acad. Sci. USA* **115** 6911–5

[12] Yagan O, Qian D, Zhang J and Cochran D 2013 Conjoining speeds up information diffusion in overlaying social-physical networks *IEEE J. Sel. Areas Commun.* **31** 1038–48

[13] Gómez S, Díaz-Guilera A, Gómez-Gardeñes J, Pérez-Vicente C J, Moreno Y and Arenas A 2013 Diffusion dynamics on multiplex networks *Phys. Rev. Lett.* **110** 028701

[14] Lazaridis F, Gross B, Maragakis M, Argyrakis P, Bonamassa I, Havlin S and Cohen R 2018 Spontaneous repulsion in the $A + B \rightarrow 0$ reaction on coupled networks *Phys. Rev.* E **97** 040301

[15] Buono C, Alvarez-Zuzek L G, Macri P M and Braunstein L A 2014 Epidemics in partially overlapped multiplex networks *PLoS One* **9** e92200

[16] Kiss I Z, Miller J C and Simon P L 2016 *Mathematics of Epidemics on Networks: From Exact to Approximate Models* (Berlin: Springer)

[17] Wang W, Tang M, Stanley H E and Braunstein L A 2017 Unification of theoretical approaches for epidemic spreading on complex networks *Rep. Prog. Phys.* **80** 036603

[18] Anderson R M and May R M 1992 *Infectious Diseases of Humans* (Oxford: Oxford University Press)

[19] Newman M E 2002 Spread of epidemic disease on networks *Phys. Rev.* E **66** 016128

[20] Meyers L 2007 Contact network epidemiology: bond percolation applied to infectious disease prediction and control *Bull. Am. Math. Soc.* **44** 63–86

[21] Kazui T and Videen S D 1982 Foreign relations during the edo period: Sakoku reexamined *J. Jpn. Stud.* **8** 283–306

[22] Guimera R, Mossa S, Turtschi A and Amaral L N 2005 The worldwide air transportation network: anomalous centrality, community structure, and cities' global roles *Proc. Natl Acad. Sci. USA* **102** 7794–9

[23] Bae J and Kim S 2014 Identifying and ranking influential spreaders in complex networks by neighborhood coreness *Physica* A **395** 549–59

[24] Liu Y, Tang M, Zhou T and Do Y 2016 Identify influential spreaders in complex networks, the role of neighborhood *Physica* A **452** 289–98

[25] Wang J, Hou X, Li K and Ding Y 2017 A novel weight neighborhood centrality algorithm for identifying influential spreaders in complex networks *Physica* A **475** 88–105

[26] Miller J C, Slim A C and Volz E M 2012 Edge-based compartmental modelling for infectious disease spread *J. R. Soc. Interface* **9** 890–906

[27] Miller J C 2018 A primer on the use of probability generating functions in infectious disease modeling *Infect. Dis. Mod.* **3** 192–248

[28] Valdez L D, Macri P A and Braunstein L A 2012 Temporal percolation of the susceptible network in an epidemic spreading *PLoS One* **7** e44188

[29] Gautreau A, Barrat A and Barthelemy M 2008 Global disease spread: statistics and estimation of arrival times *J. Theor. Biol.* **251** 509–22

[30] Stauffer D 1979 Scaling theory of percolation clusters *Phys. Rep.* **54** 1–74

[31] Leath P 1976 Cluster size and boundary distribution near percolation threshold *Phys. Rev.* B **14** 5046

[32] Havlin S and Ben-Avraham D 1987 Diffusion in disordered media *Adv. Phys.* **36** 695–798

[33] Bunde A and Havlin S 1991 *Fractals and Disordered Systems* (Berlin: Springer)

[34] Buono C, Lagorio C, Macri P and Braunstein L A 2012 Crossover from weak to strong disorder regime in the duration of epidemics *Physica* A **391** 4181–5

[35] Cohen R and Havlin S 2010 *Complex Networks: Structure, Robustness and Function* (Cambridge: Cambridge University Press)

[36] Bollobás B 2001 *The Diameter Cambridge Studies in Advanced Mathematics* 2nd edn (Cambridge: Cambridge University Press) pp 251–81

[37] Cohen R, Ben-Avraham D and Havlin S 2002 Percolation critical exponents in scale-free networks *Phys. Rev.* E **66** 036113

[38] Stauffer D and Aharony A 2014 *Introduction to Percolation Theory* 2nd edn (Boca Raton, FL: CRC Press)

[39] Hoshen J, Kopelman R and Monberg E M 1978 Percolation and cluster distribution. II. Layers, variable-range interactions, and exciton cluster model *J. Stat. Phys.* **19** 219–42

[40] Nakanishi H and Stanley H E 1978 A test of scaling near the bond percolation threshold *J. Phys.* A **11** L189

[41] https://flightradar24.com/ (Accesed: 18 July 2018)

[42] Verma T, Araújo N A and Herrmann H J 2014 Revealing the structure of the world airline network *Sci. Rep.* **4** 5638

[43] Durrett R 2007 *Random Graph Dynamics* (Cambridge: Cambridge University Press)